Superlattices and Microstructures 125 (2019) 287–294

Contents lists available at ScienceDirect

Superlattices and Microstructures

journal homepage: www.elsevier.com/locate/superlattices

Improvement of the photovoltaic performance of Ag-alloyed $Cu_2ZnSn(S,Se)_4$-based solar cells by optimizing the selenization temperature

Xiaoli Zhai[a], Bin Yao[a,b,*], Yongfeng Li[a,b,**], Zhanhui Ding[b], Rui Deng[c], Yingrui Sui[d], Haifeng Zhao[e], Ligong Zhang[e], Zhenzhong Zhang[e]

[a] State Key Lab of Superhard Materials and College of Physics, Jilin University, Changchun 130023, PR China
[b] Key Laboratory of Physics and Technology for Advanced Batteries (Ministry of Education), College of Physics, Jilin University, Changchun, 130012, PR China
[c] School of Materials Science and Engineering, Changchun University of Science and Technology, Changchun, 130022, PR China
[d] Key Laboratory of Functional Materials Physics and Chemistry of the Ministry of Education, Jilin Normal University, Siping, 136000, Jilin, PR China
[e] State Key Laboratory of Luminescence and Applications, Changchun Institute of Optics, Fine Mechanics and Physics, Chinese Academy of Sciences, No. 3888 Dongnanhu Road, Changchun, 130033, PR China

ARTICLE INFO

Keywords:
$Cu_2ZnSn(S,Se)_4$
Ag doping
Solar cell
Selenization temperature
Power conversion efficiency

ABSTRACT

$(Cu_{1-x}Ag_x)_2ZnSn(S,Se)_4$ films with Ag content of x = 0 (CZTSSe), 0.05 (CAZTSSe) and the corresponding solar cells were fabricated on soda-lime glass (SLG) substrates by sol-gel method and rapid selenization thermal processing (RTP). As Ag is alloyed into CZTSSe, Cu^+ cation in CZTSSe films was replaced by Ag^+ cation, leading to the improvement in crystal quality, the decrease of hole concentration and the increase of bandgap. We observed an increase in open-circuit voltage (V_{OC}) and an accompanying rise in device efficiency from 4.48% to 5.94% as Ag is alloyed into CZTSSe. To further improve the efficiency, we optimized the selenization temperature of the CAZTSSe films. It is found that the optimized selenization temperature is 530 °C and the best efficiency of the corresponding CAZTSSe solar cell is 7.91%. The improvement of device performance with selenization temperature is mainly attributed to the optimization of device parameters such as reversion saturation current density (J_0), diode ideal factor (A) and series resistance (R_S), which are determined by crystal quality and grain size of CAZTSSe films as well as structure of the CAZTSSe/CdS and CAZTSSe/Mo interfaces.

1. Introduction

Due to the similar crystalline structure and bandgap to $Cu(In,Ga)(S,Se)_2$ (CIGSSe) as well as superiorities of earth-abundant component elements, nontoxic and low-cost processing techniques, $Cu_2ZnSn(S,Se)_4$ (CZTSSe) with kesterite structure has attracted much attention because it is an ideal alternative of CIGS for next generation photovoltaics materials and has been studied widely recently [1–4]. However, to date the most superior photoelectric conversion efficiency (PCE) of the CZTSSe-based solar cell is only 12.6% [5], which is fall further behind 22.9% of CIGSSe solar cells [6]. The bottleneck that the PCE of CZTSSe solar cell cannot be

* Corresponding author. State Key Lab of Superhard Materials and College of Physics, Jilin University, Changchun 130023, PR China.
** Corresponding author. Key Laboratory of Physics and Technology for Advanced Batteries (Ministry of Education), College of Physics, Jilin University, Changchun, 130012, PR China.
E-mail addresses: binyao@jlu.edu.cn (B. Yao), liyongfeng@jlu.edu.cn (Y. Li).

https://doi.org/10.1016/j.spmi.2018.11.018
Received 28 September 2018; Received in revised form 19 November 2018; Accepted 28 November 2018
Available online 28 November 2018

further improved is ascribed to the large open-circuit voltage (V_{OC}) deficit ($E_g/q–V_{OC}$), which results from Fermi level pinning induced by plenty of Cu_{Zn} antisite defects [7–10]. However, theoretical researches indicate that the Cu_{Zn} antisite defect has lower formation energy than other defects, which is mainly due to the similar ionic radius and the small chemical differences between Cu and Zn [10,11]. Therefore, it is a valid method to decrease of V_{OC} deficit and improve efficiency that inhibiting the formation of Cu_{Zn} defects in CZTSSe.

Recently, Chen and Wei et al. reported that the formation energy of Ag_{Zn} antisite defects in the CAZTSSe is higher than that of Cu_{Zn} antisite defect by first-principles calculations, so partial substitution of Ag for Cu in CZTSSe can suppress formation of Cu_{Zn} defects, eliminate Fermi level pinning and thus improve V_{OC} [10,12]. Many studies have been carried out by incorporation of Ag into CZTSSe [13–17]. However, it has been proven that the electrical conductivity and crystal quality of CAZTSSe with a high concentration of Ag are always poor, which is unfavorable to develop high performance devices [15]. It is known that selenization temperature is an important parameter to control crystal quality, electrical and optical properties of CZTSSe films [18,19]. Therefore, finding an optimal selenization temperature is critical to improve the structural, electrical and optical properties of CAZTSSe as well as V_{OC} of CAZTSSe-based solar cells. However, there are few literature reported about the influence of selenization temperature on PCE of CAZTSSe solar cell.

In the present work, we prepared CZTSSe and CAZTSSe films with nominal atomic ratio of Ag/(Ag + Cu) of 5% by sol-gel spin coating technique combining with post-selenization process. The corresponding solar cells with traditional structures were also fabricated and the effect of Ag alloying and selenization temperature on performance of the devices were systematically investigated. The influencing mechanisms were suggested by analyzing the crystal quality and electrical properties of absorber layers as well as the structure and quality of absorber/emitter and absorber/back electrode interfaces. Through optimizing the selenization temperature, a CAZTSSe-based photovoltaic device with an efficiency of 7.91% was obtained.

2. Experimental methods

A clear pale yellow precursor solution of Cu_2ZnSnS_4(CZTS) was prepared by gel-sol method. Briefly, $Cu(CH_3COO)_2{\cdot}H_2O$ (8.66 mmol), $SnCl_2{\cdot}2H_2O$ (5.6 mmol), $CS(NH_2)_2$ (45 mmol), $ZnCl_2$ (6.6 mmol) and 0.2 mL neovaricaine were dissolved in 10 mL Dimethyl sulfoxide (DMSO), and followed by several hours of magnetic stirring at room temperature [20]. To obtain $(Cu_{1-x}Ag_x)_2ZnSnS_4$ (CAZTS) precursor solution with nominal atomic ratio of Ag/(Ag + Cu) of 5%, 0.45 mmol nitrate ($AgNO_3$) to substitute for part of $Cu(CH_3COO)_2{\cdot}H_2O$ (0.45 mmol) were added to the CZTS precursor solution. All the raw materials were purchased from Sinopharm Chemical Reagent. The CZTS (or CAZTS) films were prepared by spin coating the CZTS (or CAZTS) precursor solution on soda-lime glass (SLG) and Mo-coated SLG at 3000 rpm for 30 s, following by quick drying at 300 °C for 3 min on a hot plate in a glove box filled with nitrogen. The spin coating and drying procedures were repeated 10 times to get CZTS (or CAZTS) precursor films with a thickness of ~1.5 μm. Then precursor films were put into a graphite box with 150 mg selenium powder and annealed in a rapid thermal processing (RTP) furnace. The CZTS films were annealed for 11 min at 550 °C to obtain CZTSSe films, and the CAZTS films were annealed for 11 min at 510, 520, 530, 540 and 550 °C, respectively, to prepare $(Cu_{1-x}Ag_x)_2ZnSn(S,Se)_4$ (CAZTSSe) films. To fabricate solar cells with convention structure, the CdS film with a thickness of ~60 nm was prepared by chemical water bath deposition (CBD) on CZTSSe or CAZTSSe thin films, respectively. Next, a 50-nm-thick intrinsic ZnO and a 250-nm-thick ITO layers were fabricated on CdS buffer layers by radio frequency magnetron sputtering. Al electrodes (~1.0 μm) were finally deposited on the ITO layer by thermal evaporation method and the device with 0.19 cm^2 was obtained by mechanical scribing.

The crystal structures of CZTSSe and CAZTSSe films were measured using X-ray diffraction (XRD) with Cu *K*-α radiation (λ = 1.5406 Å). The structure properties of the corresponding films ware characterized by Raman spectrometer with an excitation line of 532 nm. The surface morphology of selenized films and section morphology of the devices was recorded using Scanning electron microscope (SEM, Hitachi S-4800). The element compositions of absorbers were analyzed by EDS (EDAX Genesis 2000). Hall-effect measurement system with Van der Pauw configuration was used to test electrical properties. The current density–voltage (*J–V*) curves were collected via a solar simulator (SAN-EI, XES-40S2-CE; AM 1.5) and a Keithley 2400 Source Meter. The light intensity of the solar simulator illuminated on devices is 100 mW/cm^2. The external quantum efficiency (EQE) measurements were carried out using an EQE system equipped with a lock-in amplifier (Stanford, SR830) and a light source (150 W xenon lamp). The light source was standardized with authenticated Si (300–800 nm) and InGaAs (800–1300 nm) solar cell.

3. Results and discussion

Fig. 1a displays XRD patterns of the CAZTSSe films with a nominal Ag/(Ag + Cu) of zero and 5% at a selenization temperature of 550 °C for 11 min. The XRD patterns indicate that both films have a kesterite structure [PDF 42–1120, 97-009-5117] and no secondary phases are observed. For clearly demonstrating the peak shift, the corresponding enlarged view of the (204) peaks are shown in Fig. 1b. The (204) diffraction peaks of the CAZTSSe film shows a significant shift (0.12°) towards the low angles with respect to the CZTSSe film. The compositions of the CZTSSe and CAZTSSe films are determined by EDS results, as listed in Table 1. The measured ratio of Ag/(Ag + Cu) is 5.13 is closed to nominal ratio, suggesting Ag dopants are doped into CZTSSe. It should be noted that, according to the peak shift towards the low diffraction angle, it is hard to further determine Ag substituting site because of the radius of Ag^+ (1.14 Å) larger than that of Cu^+ (0.77 Å), Zn^{2+} (0.74 Å) and Sn^{4+} (0.69 Å) [10,14,15]. In addition, smaller S atoms were partially substituted by larger Se, which also causes a 2θ shift toward the low-angle side. As listed in Table 1, the S/(S + Se) ratio is 0.059 and 0.051 for the CZTSSe and CAZTSSe, respectively. The XRD peak shift induced by such small difference in S/(S + Se) ratio can be estimated to be less than 0.01° according to the previous works [21–23]. Therefore, the large XRD peak shift is

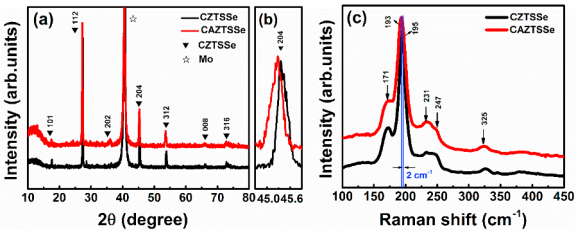

Fig. 1. (a) X-ray diffraction patterns of the selenized CZTSSe and CAZTSSe with nominal atomic ratio of Ag/(Ag + Cu) of 5% thin films at 550 °C. (b) The corresponding enlarged view of the (204) diffraction peaks in (a). (c) Raman spectra of the selenized CZTSSe and CAZTSSe thin films at 550 °C.

Table 1
Chemical compositions of the CZTSSe and CAZTSSe films selenized at 550 °C for 11 min.

Sample	Cu (at%)	Ag (at%)	Zn (at%)	Sn (at%)	Se (at%)	S (at%)	Ag/(Ag + Cu)	S/(S + Se)	Zn/Sn
CZTSSe	19.25	0	14.75	11.32	51.43	3.24	0	0.059	1.3
CAZTSSe	18.47	1.00	13.80	11.72	52.18	2.83	5.13	0.051	1.17

not related to the S/(Se + S) ratio and should be attributed to the Ag doping. Furthermore, Gautam et al. predicted that the Ag occupying Cu site has the lowest formation energy in Ag-doped Cu_2ZnSnS_4 by first-principles calculations [24]. It is deduced that Ag mainly occupies Cu site in Ag-doped $Cu_2ZnSnSe_4$. The results proved that Ag has been incorporated into CZTSSe and substituted the Cu in the CZTSSe crystal.

To further understand the effect of Ag doping on electrical properties of CZTSSe, Hall effect measurement was performed for the CZTSSe and CAZTSSe. Table 2 lists the resistivity, carrier concentration and mobility of the CZTSSe and CAZTSSe films selenized at 550 °C. Both CZTSSe and CAZTSSe show p-type conduction, but hole concentration of the CAZTSSe is one order of magnitude smaller than that of the CZTSSe. In CZTSSe, the antisite defect Cu_{Zn} and vacancy on Cu site (V_{Cu}) act as main acceptors and contribute hole to valence-band [25]. For CAZTSSe, the Ag^+ occupying the Cu^+ site increases formation energies and ionization energies of acceptor-like antisite defects (Ag_{Zn} and Cu_{Zn}) and vacancy defects (V_{Cu} and V_{Ag}) [10,26–28], resulting in the decrease of hole concentration.

Since some secondary phases, such as ZnSe, ZnS, Cu_2SnSe_3 and Cu_3SnS_4, have similar XRD profiles to kesterite CZTSSe. It is difficult to detect the secondary phases only by XRD [29–31]. Therefore, Raman scattering measurements were performed for the CZTSSe and CAZTSSe films, to rule out the presence of secondary phase. As shown in Fig. 1c, the peaks are located only at 172, 195, 231, 247 and 325 cm^{-1} [27,29]. These results demonstrate that CZTSSe and CAZTSSe films are single kesterite phase and contain have a small amount of S, in agreement with the results of Table 1.

To further study the influence of Ag doped in absorber layer on the performance of CZTSSe devices. We fabricated two groups of solar cells with the same selenization condiction (at 550 °C for 11 min), in which the absorber layers are CZTSSe and CAZTSSe, respectvilely. Each group includes 8 solar cells. Fig. 2a reveals the *J–V* curves of the CZTSSe and CAZTSSe cells with the highest PCE. The performance parameters of the both solar cells, including open-circuit voltage (V_{OC}), short-circuit current density (J_{SC}), fill factor (FF) and PCE, are listed in the insert of Fig. 2a. For comparison, we also list the average parameters of the two groups of solar cells in the parentheses. The highest PCE of the solar cells increases from 4.84% to 5.94% as Ag is alloyed into CZTSSe. The increment in PCE derives mainly from the increase of V_{OC} and FF.

With an aim to further understand mechanism of the increased V_{OC} and FF, bandgaps of the CAZTSSe and CZTSSe solar cells with the highest PCE were determined by measuring EQE. Fig. 2b shows the EQE of the two solar cells with the highest PCE. The inset shows the determination of bandgaps. The bandgaps of the CZTSSe and CAZTSSe films are estimated to be 1.050, 1.072 eV, respectively. The change of bandgaps are small due to low doping concentration, which are in consistent with the previous report [29]. The electrical parameters, such as series resistance (R_S), shunt resistance (R_{Sh}), diode ideality (A) and reverse current (J_0), were calculated by processing the *J–V* curves of devices with the Sites' method [32], as listed in Table 3. The results show that Ag-substituted samples could obviously increase R_{Sh} and decrease R_S and finally contributed to a higher FF. And combination with EQE, it can be seen that the substitution of Cu by Ag improves the EQE over a broad spectral region from 600 nm to 1100 nm. It should be

Table 2
Electrical properties of the CZTSSe selenized at 550 °C and CAZTSSe thin films with different selenization temperatures.

Sample	Resistivity (Ω·cm)	Type	Carrier concentration (cm^{-3})	Mobility ($cm^2V^{-1}s^{-1}$)
CZTSSe-550 °C	1.7×10^2	p	3.1×10^{16}	1.2
CAZTSSe-510 °C	8.3×10^2	p	6.1×10^{15}	1.3
CAZTSSe-520 °C	6.7×10^2	p	3.9×10^{15}	2.4
CAZTSSe-530 °C	5.1×10^2	p	3.6×10^{15}	3.5
CAZTSSe-540 °C	5.5×10^2	p	3.4×10^{15}	3.4
CAZTSSe-550 °C	6.5×10^2	p	4.9×10^{15}	2.0

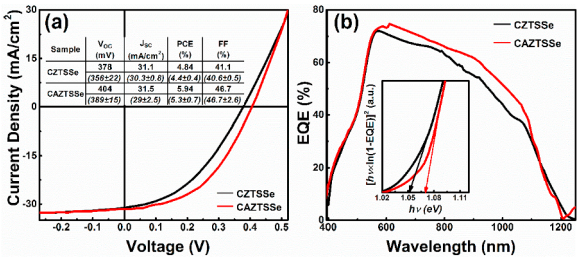

Fig. 2. (a) Current – voltage characteristics of the CZTSSe and CAZTSSe solar cell selenized at 550 °C under AM1.5G illumination. The inserted table in (a) lists the parameters of V_{OC}, J_{SC}, FF and PCE. The cell parameters are the best cell performances and the average values are based on 8 Solar Cells (Marked in Italic). (b) EQE of the CZTSe and CAZTSSe solar cells devices. The insert shows the bandgap determined by the $[h\nu \times \ln(1\text{-EQE})]^2$ vs $h\nu$ curve.

Table 3
R_S, R_{Sh}, A, and J_0 of the CZTSSe and CAZTSSe solar cell with CZTSSe and CAZTSSe absorber layer selenized at 550 °C for 11 min.

Sample	R_{Sh} (Ω cm^2)	R_S (Ω cm^2)	A	J_0 (mA/cm^2)
CZTSSe-550 °C	492	3.32	2.64	0.120
CAZTSSe-550 °C	571	2.35	2.29	0.045

noted that Ag-substituting Cu site can suppress recombination and improve hole collection at the absorber/Mo interface, which consistent with the variation of J_0. The decrease of the carrier concentration in absorber layer via Ag-doping leads to the enlargement of space charge region of the absorber to enhance carrier collection, which make EQE improved. It is known that the V_{OC} can expressed as under ideal conditions:

$$V_{oc} \approx \frac{AkT}{q} ln\frac{J_L}{J_0} = \frac{AkT}{q}(lnJ_L - lnJ_{00} + \frac{E_g}{kT}) \quad (1)$$

where $J_0 = J_{00}\exp(-E_g/kT)$, J_{00} is prefactor of J_0, J_L, k, q, T and E_g are photocurrent density, Boltzmann constant, electron charge, temperature and bandgap of absorber layer, respectively. Usually, it is considered $J_L \approx J_{SC}$. Using Eq (1) and the J_{SC}, J_0 and E_g of the CZTSSe and CAZTSSe solar cell, the increased V_{OC} of CAZTSSe solar cell derives from the increase in E_g induced by Ag alloying, while the increased FF due to R_S and R_{Sh}.

For improving PCE of the CAZTSSe solar cell, we optimized crystalline quality of the CAZTSSe films by changing selenization temperatures. Fig. 3a and b shows the XRD patterns and Raman scattering spectra of the CAZTSSe films selenized at 510, 520, 530, 540 and 550 °C, respectively. It is found that all CAZTSSe films are single phase with a kesterite structure. Compositions of the CAZTSSe films were measured by EDS, as listed in Table 4. For all CAZTSSe films, the atomic ratios of Ag/(Ag + Cu) are closed to the nominal ratio of 5%, indicating that no content loss of Ag occurs during the selenization processes.

We preapred five CAZTSSe solar cells with the conventional structure (SLG/Mo/CAZTSSe/CdS/i-ZnO/ITO/Al) using CAZTSSe as the absorber. To study influence of selenization temperature on PCE, the *J–V* curves of the solar cells were recorded under AM1.5 G illuminations, as shown in Fig. 4a. The J_{SC}, V_{OC}, FF and PCE are listed in the insert of Fig. 4a. When the selenization temperature decreases from 550 to 530 °C, the PCE increases from 5.94% to 7.91%. Then the PCE decreases to 5.51% as the temperature reduces to 510 °C. The variation of the V_{OC}, J_{SC} and FF with the selenization temperature is similar to that of the PCE, indicating that the variation of PCE is contributed from the variation of the V_{OC}, J_{SC} and FF. The analysis above indicates that the optimized selenization temperature for the Ag-doped CZTSSe was 530 °C, which is consistent with the previous reports that the lower optimized selenization temperature is necessary for Ag-doped CZTSSe [29,33]. The difference in selenization temperature is of significant for improving efficiency of solar cells via post-selenization processing.

Fig. 4b shows EQE spectra of the five CAZTSSe devices. For calculating the bandgap of the absorber layers in CAZTSSe devices, we

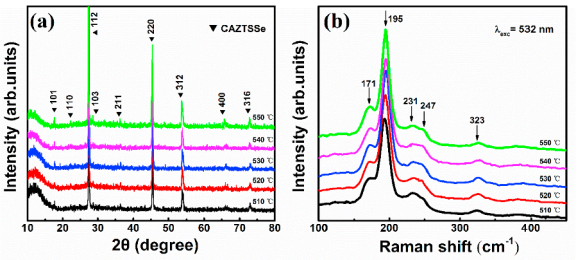

Fig. 3. (a) X-ray diffraction pattern and (b) Raman spectra for the selenizated CAZTSSe thin films with different selenization temperature.

Table 4
Chemical compositions of the CAZTSSe films selenized at various temperature.

T (°C)	Cu (at%)	Ag (at%)	Zn (at%)	Sn (at%)	Se (at%)	S (at%)	Ag/(Ag + Cu)
510	19.28	1.14	13.67	12.62	50.32	2.97	5.5
520	18.15	0.99	14.46	11.56	51.84	3.0	5.17
530	18.68	1.09	14.19	12.21	50.22	3.62	5.51
540	19.41	0.99	14.56	12.37	49.64	3.03	4.85
550	18.47	1.00	13.80	11.72	52.18	2.83	5.13

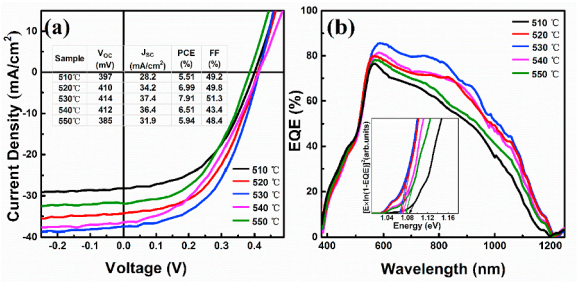

Fig. 4. (a) Current−voltage characteristics of the CAZTSSe-based solar cell using the CAZTSSe absorber layer prepared at different selenization temperatures of 510, 520, 530, 540 and 550 °C under AM 1.5G illumination and the corresponding parameters of V_{OC}, J_{SC}, FF and PCE are listed in the inserted table. (b) EQE of the CAZTSSe solar cells devices. The insert shows the determined of bandgap by the $[h\nu \times \ln(1\text{-EQE})]^2$ vs $h\nu$ curve.

plotted $[h\nu \times \ln(1\text{-EQE})]^2$ versus photon energy ($h\nu$), as shown in the insert of Fig. 4b. The bandgaps of the five CAZTSSe absorber layers are respectively determined to be 1.083, 1.071, 1.061, 1.063 and 1.072 eV. It is known from Eq (1) that V_{OC} is related to J_{SC}, J_0 (or J_{00}) and E_g and is proportional to E_g. However, the change of the V_{OC} with selenization temperature is not similar to that of the E_g. For example, among the five solar cells, the E_g is the lowest for the CAZTSSe prepared at 530 °C, but its V_{OC} is the largest, while E_g is the highest for the CAZTSSe prepared at 510 °C, its V_{OC} is not the largest but the lowest. These results indicate that the differences in open circuit voltage of the CAZTSSe devices are not derived from the differences in bandgap but in J_{SC} and J_0.

It can be deduced from Fig. 4b that differences between the J_{SC} for the CAZTSSe solar cells mainly derives from differences in photocurrent density J_L and electrical parameters including R_S, R_{Sh}, A and J_0, which are calculated and listed in Table 5. It is well known that the J_{SC} equation can be expressed as:

$$(1 + R_s/R_{Sh})J_{SC} = J_L - J_0(e^{\frac{qR_S J_{SC}}{AkT}} - 1) \quad (2)$$

Since the R_S/R_{Sh} is between 0.002 and 0.007, much less than 1, its influence on the J_{SC} can be neglected. It is known that J_L is related to depletion region width (W_d) of solar cell, which is determined by hole concentration of the absorber. The hole concentration of the CAZTSSe and CZTSSe absorbers were characterized by Hall effect, as exhibited in Table 2. It can be found that the hole concentration decreases with selenization temperature increases from 510 to 530 °C firstly and then increases slightly from 530 to 550 °C. The former make the W_d increase, leading to increment of J_L, while latter makes the W_d decrease slightly, resulting in decrease in J_L. The change of the J_L with the temperature is similar to that of the J_{SC}. So, it is deduced that the difference J_{SC} is affect by the difference in the J_L. But the influence is little due to very small difference in the hole concentration of the CAZTSSe films. Based on the differences in J_0 and R_S/A of the solar cells, we can conclude that the difference in the J_{SC} mainly comes from the difference in J_0 and R_S/A. From Eq (2), it can be seen that the current density increases with the decrease of R_S/A, which values are shown in Table 5. In these devices, the R_S/A is the lowest for the CAZTSSe prepared at 530 °C and its J_{SC} is the largest, which results are consistent with Eq (2). Fig. 5 shows a plot of FF as a function of R_S for the CAZTSSe solar cells. The FF decreases with the increasing of R_S, suggesting that the FF is strongly associated with the R_S. According to the analysis above, we conclude that the variation of the V_{OC}, J_{SC} and FF with the selenization temperature is mainly ascribed to the change of the J_0, A and R_S.

As we all know, J_0, A and R_S are related to crystal quality and structure of absorber and of absorber/emitter and absorber/back

Table 5
R_{Sh}, R_S, R_S/R_{Sh}, A, R_S/A and J_0 of the CAZTSSe solar cell using CAZTSSe absorber layer prepared at the selenization temperature of 510 °C, 520 °C, 530 °C, 540 °C and 550 °C in the periods of 11 min under AM 1.5G Illumination.

Sample	R_{Sh} (Ω cm²)	R_S (Ω cm²)	A	J_0 (mA/cm²)	R_S/R_{Sh}	Rs/A (Ω cm²)
CAZTSSe-510 °C	476	2.37	2.31	0.040	0.0049	1.02
CAZTSSe-520 °C	515	2.23	2.20	0.035	0.0043	1.01
CAZTSSe-530 °C	540	1.60	2.23	0.030	0.0028	0.65
CAZTSSe-540 °C	531	2.98	2.28	0.039	0.0056	1.30
CAZTSSe-550 °C	571	2.35	2.29	0.045	0.0041	1.03

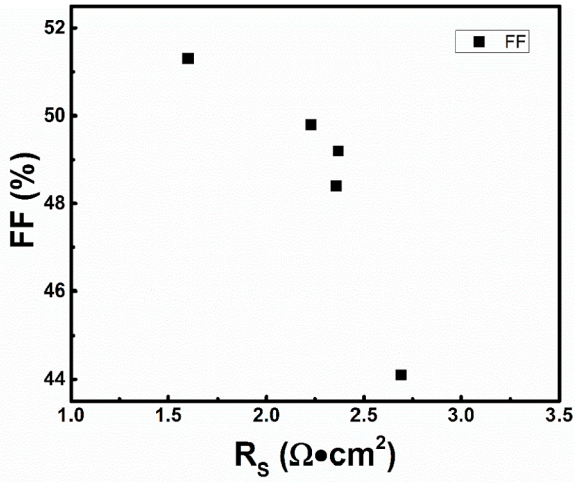

Fig. 5. The relationship between FF and Rs at selenization temperatures of 510, 520, 530, 540 and 550 °C, respectively.

electrode interfaces [18]. Fig. 6a–e and f-j show SEM images of the surface morphology of CAZTSSe films prepared at various selenization temperatures and of the corresponding cross-section morphology of corresponding CAZTSSe solar cells. For the CAZTSSe films obtained at 510 and 520 °C, as shown in Fig. 6a and b, the surfaces are smoothing and composed of grains with larger size, but there are many pin-holes at the surfaces, which will form traps at the interface of CdS/CAZTSSe. These traps make photogenerated electron and hole recombine, and result in enlargement of J_0. As shown in Fig. 6f and g, the bulk of the two CAZTSSe films consist of two layers. The top layer is larger grains, while bottom layer is of smaller grains [18,34]. In addition, there are some pin-holes in the bulks. It is demonstrated that the interface form by the CZTSSe with smaller grains and back electrode Mo will increase recombination rate of J_0 compared to the interface formed by the Mo and CAZTSSe with large grains [18]. In addition, the pin-holes and small grains will increase R_S [18,32]. When selenization temperature is 530 °C, the surface of the CAZTSSe film is smoothing and compact, moreover, has not any pin-hole. The grains in the bulk are large, stack densely and contact well with back electrode, as shown in Fig. 6c and h. These features result in decrease in J_0 and R_S compared to those of the solar cells with CAZTSSe absorber prepared at 510 and 520 °C. Further increasing the selenization temperature, although the grain size increases, there will pin-holes appear in the bulk, as shown in Fig. 6i and f. These lead to increase in the J_0 and R_S with increasing temperature.

It is noted that there are a layer of $MoSe_2$ at between the CAZTSSe and Mo, which is due to the reaction of Mo with Se in the selenization processes [34,35]. It is demonstrated that the $MoSe_2$ will promote recombination and make the recombination at CAZTSSe/Mo interface become dominant. It is known from Table 5 that the A is larger than 2 for all of the CAZTSSe solar cells [36,37]. The $MoSe_2$ also increases R_S [18,35]. The thickness of $MoSe_2$ layers was determined to be 25, 35, 43, 38 and 70 nm, respectively, as labeled in Fig. 6. It has been reported that the effect of $MoSe_2$ thickness on performance of solar cells is slight as the thickness is below ~200 nm. Even, for the thicker $MoSe_2$ (e.g. thickness of ~1000 nm), efficiency of solar cell is still beyond 10% [38,39]. Therefore, the $MoSe_2$ layers with the thicknesses of less than 100 nm has little impact on solar cells in our present experiments.

Based on the discussion above, we concluded that the change of the J_0, A and R_S with selenizaiton temperature is derived from change of crystal quality and grain size of surface and bulk of CAZTSSe films, and can be optimized by tuning selenization temperature.

4. Conclusion

In summary, the single-phase kesterite undoped and Ag-doped CZTSSe films were prepared by using DMSO-based solution and selenization in the temperature ranging from 510 to 550 °C. It is demonstrated that the Ag^+ ion substitutes for Cu^+ ion in CZTSSe to

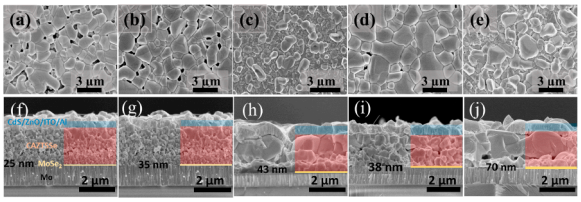

Fig. 6. The surface SEM images of CAZTSSe thin films prepared at different selenization temperatures and cross-sectional images of the corresponding CAZTSSe solar cells devices: (a,f) 510 °C, (b,g) 520 °C, (c,h) 530 °C, (d,i) 540 °C and (e,j) 550 °C. The thickness values of $MoSe_2$ was described in the Fig. 6.

form CAZTSSe, which leads to decrease in hole concentration of the CAZTSSe film. Ag alloying makes PCE increase from 4.48% of CZTSSe solar cell to 5.94% of CAZTSSe. The increased PCE is mainly due to increase in the V_{OC} and FF, which derive from E_g, R_S and R_{Sh}. The PCE changes with the selenizaiton temperature, and the PCE reaches to 7.91% in the solar cell with the CAZTSSe layer prepared at 530 °C. It is demonstrated that the variation of the PCE with selenization temperature is primarily attributed to J_0, A and R_S, which are determined by crystal quality and grain size of CAZTSSe films as well as strucutre of the CAZTSSe/CdS and CAZTSSe/Mo interfaces.

Acknowledgement

This work is supported by the National Natural Science Foundation of China under Grant Nos. 61774075, 11274135, 61604029 and 61505067, The Science and Technology Development Project of Jilin Province under grant No. 20170101142JC, Specialized Research Fund for the Doctoral Program of Higher Education under Grant No. 20130061130011, and Ph.D. Programs Foundation of Ministry of Education of China under Grant No. 20120061120011. This work was also supported by Graduate Innovation Fund of Jilin University (No. 2017051) and High Performance Computing Center of Jilin University, China.

References

[1] D.B. Mitzi, O. Gunawan, T.K. Todorov, K. Wang, S. Guha, The path towards a high-performance solution-processed kesterite solar cell, Sol. Energy Mater. Sol. Cells 95 (6) (2011) 1421–1436.
[2] W. Ki, H.W. Hillhouse, Earth-abundant element photovoltaics directly from soluble precursors with high yield using a non-toxic solvent, Adv. Energy Mater. 1 (5) (2011) 732–735.
[3] G. Wang, W. Zhao, Y. Cui, Q. Tian, S. Gao, L. Huang, D. Pan, Fabrication of a $Cu_2ZnSn(S,Se)_4$ photovoltaic device by a low-toxicity ethanol solution process, ACS Appl. Mater. Interfaces 5 (20) (2013) 10042–10047.
[4] C.M. Fella, Y.E. Romanyuk, A.N. Tiwari, Technological status of $Cu_2ZnSn(S,Se)_4$ thin film solar cells, Sol. Energy Mater. Sol. Cells 119 (2013) 276–277.
[5] W. Wang, M.T. Winkler, O. Gunawan, T. Gokmen, T.K. Todorov, Y. Zhu, D.B. Mitzi, Device characteristics of CZTSSe thin-film solar cells with 12.6% efficiency, Adv. Energy Mater. 4 (7) (2014) 1301465.
[6] M.A. Green, Corrigendum to 'Solar cell efficiency tables (version 49)', Prog. Photovoltaics Res. Appl. 25 (2017) 3–13 Progress in Photovoltaics: Research and Applications, 25 (2017) 333-334.
[7] O.G. Kong Fai Tai, Masaru Kuwahara, Shi Chen, Subodh Gautam Mhaisalkar, a.D.B.M, Cheng hon alfred huan fill factor losses in $Cu_2ZnSn(S_xSe_{1-x})_4$ solar cells: insights from physical and electrical characterization of devices and exfoliated films, Adv. Energy Mater 6 (2016) 1501609.
[8] S. Siebentritt, S. Schorr, Kesterites-a challenging material for solar cells, Prog. Photovoltaics Res. Appl. 20 (2012) 512–519.
[9] S. Bourdais, C. Choné, B. Delatouche, A. Jacob, G. Larramona, C. Moisan, A. Lafond, F. Donatini, G. Rey, S. Siebentritt, A. Walsh, G. Dennler, Is the Cu/Zn disorder the main culprit for the voltage deficit in kesterite solar cells? Adv. Energy Mater. 6 (12) (2016) 1502276.
[10] Z.-K. Yuan, S. Chen, H. Xiang, X.-G. Gong, A. Walsh, J.-S. Park, I. Repins, S.-H. Wei, Engineering solar cell absorbers by exploring the band Alignment and defect disparity: the case of Cu- and Ag-based kesterite compounds, Adv. Funct. Mater. 25 (43) (2015) 6733–6743.
[11] S. Chen, A. Walsh, X.G. Gong, S.H. Wei, Classification of lattice defects in the kesterite Cu_2ZnSnS_4 and $Cu_2ZnSnSe_4$ earth-abundant solar cell absorbers, Adv. Mater. 25 (11) (2013) 1522–1539.
[12] D. Shin, B. Saparov, D.B. Mitzi, Defect engineering in multinary earth-abundant chalcogenide photovoltaic materials, Adv. Energy Mater. 7 (11) (2017) 1602366.
[13] W. Li, X. Liu, H. Cui, S. Huang, X. Hao, The role of Ag in $(Ag,Cu)_2ZnSnS_4$ thin film for solar cell application, J. Alloy. Comp. 625 (2015) 277–283.
[14] C.J. Hages, M.J. Koeper, R. Agrawal, Optoelectronic and material properties of nanocrystal-based CZTSe absorbers with Ag-alloying, Sol. Energy Mater. Sol. Cell. 145 (2016) 342–348.
[15] T. Gershon, K. Sardashti, O. Gunawan, R. Mankad, S. Singh, Y.S. Lee, J.A. Ott, A. Kummel, R. Haight, Photovoltaic device with over 5% efficiency based on an n-type $Ag_2ZnSnSe_4$ absorber, Adv. Energy Mater. 6 (10) (2016) 1601182.
[16] A. Guchhait, Z. Su, Y.F. Tay, S. Shukla, W. Li, S.W. Leow, J.M.R. Tan, S. Lie, O. Gunawan, L.H. Wong, Enhancement of open-circuit voltage of solution-processed Cu_2ZnSnS_4 solar cells with 7.2% efficiency by incorporation of silver, ACS Energy Lett. 1 (6) (2016) 1256–1261.
[17] X.H. Yun Zhao, Bin Xu, Li Wen, Jian Li, Jiajia Li, Min Wang, Chen Dong, Peng Ju, Junshuai Li, Enhancing open-circuit voltage of solution-processed $Cu_2ZnSn(S,Se)_4$ solar cells with Ag substitution, IEEE J. Photovoltaics 05 (2017) 874–881.
[18] Z.Y. Xiao, B. Yao, Y.F. Li, Z.H. Ding, Z.M. Gao, H.F. Zhao, L.G. Zhang, Z.Z. Zhang, Y.R. Sui, G. Wang, Influencing mechanism of the selenization temperature and time on the power conversion efficiency of $Cu_2ZnSn(S,Se)_4$-Based solar cells, ACS Appl. Mater. Interfaces 8 (27) (2016) 17334–17342.
[19] S.A. Vanalakar, S.W. Shin, G.L. Agawane, M.P. Suryawanshi, K.V. Gurav, P.S. Patil, J.H. Kim, Effect of post-annealing atmosphere on the grain-size and surface morphological properties of pulsed laser deposited CZTS thin films, Ceram. Int. 40 (9) (2014) 15097–15103.
[20] H. Xin, J.K. Katahara, I.L. Braly, H.W. Hillhouse, 8% efficient $Cu_2ZnSn(S,Se)_4$ solar cells from redox equilibrated simple precursors in DMSO, Adv. Energy Mater. 4 (11) (2014) 1301823.
[21] P.M.P. Salomé, J. Malaquias, P.A. Fernandes, M.S. Ferreira, A.F. da Cunha, J.P. Leitão, J.C. González, F.M. Matinaga, Growth and characterization of $Cu_2ZnSn(S,Se)_4$ thin films for solar cells, Sol. Energy Mater. Sol. Cell. 101 (2012) 147–153.
[22] D.-K. Hwang, B.-S. Ko, D.-H. Jeon, J.-K. Kang, S.-J. Sung, K.-J. Yang, D. Nam, S. Cho, H. Cheong, D.-H. Kim, Single-step sulfo-selenization method for achieving low open circuit voltage deficit with band gap front-graded $Cu_2ZnSn(S,Se)_4$ thin films, Sol. Energy Mater. Sol. Cell. 161 (2017) 162–169.
[23] J. Li, R. Yao, C. Xiong, Y. Liu, K. Geng, $Cu_2ZnSn(S,Se)_4$ thin films preparation by using ammonium polysulfoselenide-based ink, Mater. Lett. 210 (2018) 20–22.
[24] G. Sai Gautam, T.P. Senftle, E.A. Carter, Understanding the effects of Cd and Ag doping in Cu_2ZnSnS_4 solar cells, Chem. Mater. 30 (14) (2018) 4543–4555.
[25] D. Han, Y.Y. Sun, J. Bang, Y.Y. Zhang, H.-B. Sun, X.-B. Li, S.B. Zhang, Deep electron traps and origin ofp-type conductivity in the earth-abundant solar-cell material Cu_2ZnSnS_4, Phys. Rev. B 87 (15) (2013) 155206.
[26] J. Kumar, S. Ingole, Structural and optical properties of $(Ag_xCu_{1-x})2ZnSnS_4$ thin films synthesised via solution route, J. Alloy. Comp. 727 (2017) 1089–1094.
[27] Y. Jiang, B. Yao, Y. Li, Z. Ding, H. Luan, J. Jia, Y. Li, K. Shi, Y. Sui, B. Zhang, Structure, optical and electrical properties of $(Cu_{1-x}Agx)_2ZnSn(S,Se)_4$ alloy thin films for photovoltaic application, Mater. Sci. Semicond. Process. 81 (2018) 54–59.
[28] S. Chen, J.-H. Yang, X.G. Gong, A. Walsh, S.-H. Wei, Intrinsic point defects and complexes in the quaternary kesterite semiconductor Cu_2ZnSnS_4, Phys. Rev. B 81 (24) (2010) 245204.
[29] Y.-F. Qi, D.-X. Kou, W.-H. Zhou, Z.-J. Zhou, Q.-W. Tian, Y.-N. Meng, X.-S. Liu, Z.-L. Du, S.-X. Wu, Engineering of interface band bending and defects elimination via a Ag-graded active layer for efficient $(Cu,Ag)_2ZnSn(S,Se)_4$ solar cells, Energy Environ. Sci. 10 (11) (2017) 2401–2410.
[30] H. Xie, Y. Sanchez, S. Lopez-Marino, M. Espindola-Rodriguez, M. Neuschitzer, D. Sylla, A. Fairbrother, V. Izquierdo-Roca, A. Perez-Rodriguez, E. Saucedo, Impact of Sn(S,Se) secondary phases in $Cu_2ZnSn(S,Se)_4$ solar cells: a chemical route for their selective removal and absorber surface passivation, ACS Appl. Mater. Interfaces 6 (15) (2014) 12744–12751.
[31] Y. Wu, Y. Zhang, Y. Sui, Z. Wang, S. Lv, M. Wei, Y. Sun, B. Yao, X. Liu, L. Yang, Bandgap engineering of $Cu_2In_xZn_{1-x}Sn(S,Se)_4$ alloy films for photovoltaic applications, Ceram. Int. 44 (2) (2018) 1942–1950.
[32] G. Yang, Y.-F. Li, B. Yao, Z.-H. Ding, R. Deng, H.-F. Zhao, L.-G. Zhang, Z.-Z. Zhang, Improvement of the photovoltaic performance of $Cu_2ZnSn(S_xSe_{1-x})_4$ solar

cells by adding polymer in the precursor solution, J. Phys. Appl. Phys. 51 (10) (2018) 105103.
[33] W.-C. Huang, S.-Y. Wei, C.-H. Cai, W.-H. Ho, C.-H. Lai, The role of Ag in aqueous solution processed $(Ag,Cu)_2ZnSn(S,Se)_4$ kesterite solar cells: antisite defect elimination and importance of Na passivation, J. Mater. Chem. 6 (2018) 15170–15181.
[34] G. Yang, Y.-F. Li, B. Yao, Z.-H. Ding, R. Deng, H.-F. Zhao, L.-G. Zhang, Z.-Z. Zhang, Growth of large grain-size $Cu_2ZnSn(S_xSe_{1-x})_4$ thin films by annealing precursors sputtered from a single quaternary target for solar cells application, Superlattice. Microst. 109 (2017) 480–489.
[35] J. Li, Y. Zhang, W. Zhao, D. Nam, H. Cheong, L. Wu, Z. Zhou, Y. Sun, A temporary barrier effect of the alloy layer during selenization: tailoring the thickness of $MoSe_2$ for efficient $Cu_2ZnSnSe_4$ solar cells, Adv. Energy Mater. 5 (9) (2015) 1402178.
[36] H. Young Park, D. Gwon Moon, J. Ho Yun, S.K. Ahn, K.H. Yoon, S. Ahn, Efficiency limiting factors in $Cu(In,Ga)Se_2$ thin film solar cells prepared by Se-free rapid thermal annealing of sputter-deposited Cu-In-Ga-Se precursors, Appl. Phys. Lett. 103 (26) (2013) 263903.
[37] G. Brammertz, M. Buffière, S. Oueslati, H. ElAnzeery, K. Ben Messaoud, S. Sahayaraj, C. Köble, M. Meuris, J. Poortmans, Characterization of defects in 9.7% efficient $Cu_2ZnSnSe_4$-CdS-ZnO solar cells, Appl. Phys. Lett. 103 (26) (2013) 163904.
[38] T. Taskesen, J. Neerken, J. Schoneberg, D. Pareek, V. Steininger, J. Parisi, L. Gütay, Device characteristics of an 11.4% CZTSe solar cell fabricated from sputtered precursors, Adv. Energy Mater. 8 (2018) 1703295.
[39] T.A. Thomas Schnabel, Theresa M. Friedlmeier, Erik Ahlswede, Solution-based preparation of $Cu_2ZnSn(S,Se)_4$ for solar cells—comparison of $SnSe_2$ and elemental Se as chalcogen source, IEEE J. Photovoltaics 2 (2015) 670–675.